J. Fluid Mech. (1979), *vol.* 92, *part* 4, *pp.* 643–657
Printed in Great Britain

Flow separation on a spheroid at incidence

By TAEYOUNG HAN AND V. C. PATEL
Institute of Hydraulic Research, University of Iowa, Iowa City

(Received 28 November 1977 and in revised form 20 July 1978)

Surface streamline patterns on a spheroid have been examined at several angles of attack. Most of the tests were performed at low Reynolds numbers in a hydraulic flume using coloured dye to make the surface flow visible. A limited number of experiments was also carried out in a wind tunnel, using wool tufts, to study the influence of Reynolds number and turbulent separation. The study has verified some of the important qualitative features of three-dimensional separation criteria proposed earlier by Maskell, Wang and others. The observed locations of laminar separation lines on a spheroid at various incidences have been compared with the numerical solutions of Wang and show qualitative agreement. The quantitative differences are attributed largely to the significant viscous–inviscid flow interaction which is present, especially at large incidences.

1. Introduction

In two-dimensional steady flow, the point of flow detachment or separation from the surface coincides with the point at which the wall shear stress vanishes. This point is characterized by a number of other features which occur concurrently. Among these, (*a*) the boundary layer thickens rapidly ahead of this point, leading to a gradual breakdown of the boundary-layer approximations and the assumption that the wall pressure distribution conforms with that given by potential-flow theory, (*b*) the first-order boundary-layer equations become singular at this point, and (*c*) the flow near the surface is reversed, so that the flow downstream of this point becomes inaccessible to usual boundary-layer analysis. The coincidence of all these phenomena in two-dimensional steady flow is well recognized, although the condition of zero wall shear stress is the criterion most often used for separation in practical boundary-layer calculation procedures.

In three-dimensional steady flow, on the other hand, the definition of the term 'separation' is not precise since the limiting behaviour of the equations has not been studied in any detail, and it is generally observed that flow detachment from the surface is not simply related to the characteristics of the flow near the surface. Specifically, flow detachment or separation is rarely associated with the vanishing of the wall shear stress except in certain special cases or at isolated points. More frequently, the shear stress remains finite on separation lines and may even be relatively large. From an engineering standpoint, however, it is essential to identify the occurrence of separation and assess its aerodynamic or hydrodynamic consequences. As the issue is judged at the present time, it appears that this would require a comprehensive examination of the overall flow field rather than the flow close to the surface alone.

0022-1120/79/4146-6900 $02.00

Yet, in most previous studies concerning separation in three dimensions, attention has been confined to the correlation of separation with observations of surface streamlines (or skin-friction lines). Among the proposed definitions of separation lines are:

(*a*) lines on which some component of the wall shear stress vanishes;

(*b*) limiting streamlines joining 'singular' points;

(*c*) the envelope of limiting streamlines;

(*d*) lines dividing flow coming from different regions.

By taking specific examples, it is readily shown that each of these is valid under certain conditions, but none is universally valid, and that flow detachment from the surface may be accompanied by one or more of these surface flow features.

The pioneering work of Maskell (1955) still represents a major milestone in the area of three-dimensional separation. On the basis of surface flow diagnostics, he identified two basic types of separation: bubble type and free-vortex type. The former is also termed 'singular separation' since the separation line passes through or joins singular points at which the wall shear stress vanishes. Separation in two-dimensional and axisymmetric flow is of this type. Such a separation line also divides flows coming from different regions (i.e. upstream and downstream), so that the flow beyond it is not accessible to boundary-layer analysis. The free-vortex or 'ordinary' separation does not involve singular points and is recognized only by surface streamlines coming together along some line and leaving the surface along it. Here, flow detachment from the surface is usually accompanied by the formation of a longitudinal vortex. Also, as first pointed out by Wang (1972), the flow on either side of such a line appears to come from a common upstream origin and therefore there is no implication of inaccessibility from upstream.

Wang (1972) has adopted the separation models of Maskell to describe the flow past bodies of revolution at incidence and introduced the concepts of 'open' and 'closed' separations, similar to the free-vortex and bubble separations of Maskell. An open separation line is akin to the free-vortex separation line of Maskell and does not cross the plane of symmetry of the body. Thus the flow on either side of it is fed entirely from upstream. Wang (1972, 1974*b*) further suggested that, although such a separation line runs close to the locus of points of zero circumferential component of wall shear stress, the two lines do not, in general, coincide. As we shall see later, the precise origin of an open separation line cannot be defined with certainty. A closed separation line, on the other hand, is one which forms a closed curve around the body, passing through the singular points, and is therefore identical with the bubble type of separation of Maskell. At least two singular points can be identified readily on a body of revolution at incidence, since they lie on the plane of symmetry, one on the windward and one on the leeward side, and demarcate local flow reversal. The existence of additional singular points can be established with the help of the topological law discussed by Lighthill (1963), provided certain other features of the overall flow pattern are established *a priori*. This aspect is clarified in the subsequent text. For the present, we note that a closed or bubble-separation line divides the flow coming from upstream from that appearing to originate from downstream.

Many of the concepts reviewed here have not received detailed experimental confirmation, although Stetson (1972), Zakkay, Miyazawa & Wang (1974) and others have provided some evidence in support of the open-separation concept of Wang (see Wang 1976 for further discussion). A detailed experimental programme was

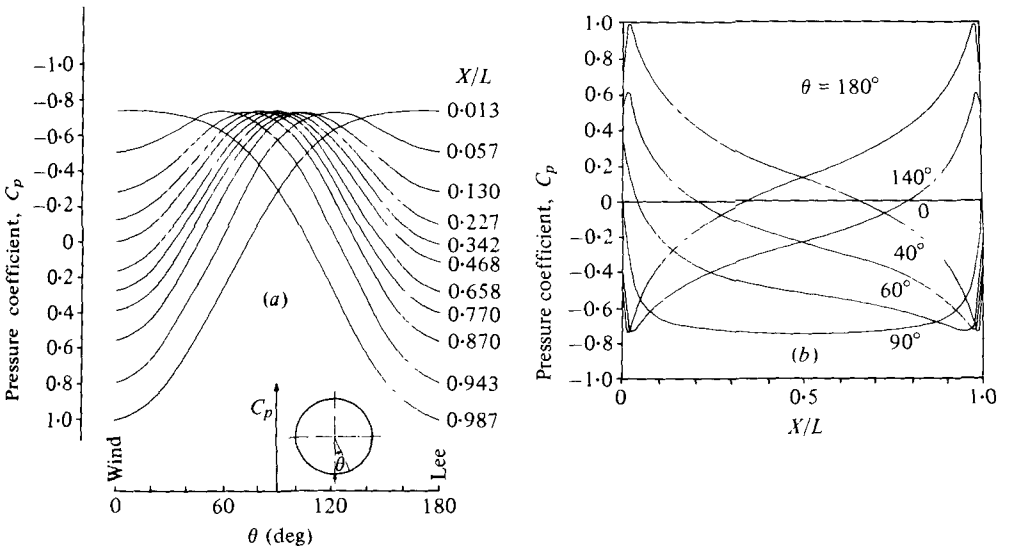

FIGURE 1. Potential-flow pressure distribution on a 4·3:1 spheroid at 30° incidence. (*a*) Circumferential. (*b*) Longitudinal.

therefore planned to make mean-flow and turbulence measurements in the three-dimensional boundary layer on a representative shape in order to provide quantitative data on boundary-layer development, as well as to establish criteria for separation that can be readily incorporated in modern computation procedures. The study reported here was conceived as a preliminary visual investigation in which the primary objective was to identify the basic overall features of the flow so that the proper body shape, regions for detailed boundary-layer explorations and necessary instrumentation could be chosen. The results of the study, however, go well beyond meeting these primary objectives and should be of wider interest since they appear to confirm several aspects of models of three-dimensional flow separation proposed in recent years. Although the study included three different shapes, only the results of the spheroid tests are discussed here since some theoretical information on this shape is available from the computations of Wang (1970, 1974*b*). The remaining results are discussed in Han & Patel (1977).

2. Preview of the flow past a spheroid at incidence

The potential-flow pressure distribution on the surface of a prolate spheroid of axis ratio 4·3 at an incidence of 30° is shown in figure 1, and the corresponding surface streamlines are shown in figure 2. Observe that, in the axial direction, there is a prolonged favourable pressure gradient on the windward side and a similar adverse pressure gradient on the leeward side. In the circumferential direction, the pressure gradient from the windward to the leeward side is favourable over the front half of the body and adverse over the rear half. Since the boundary layer develops under the influence of this pressure field, at least in regions where there is no separation, it enables one to surmise the possible behaviour of the boundary layer.

Along the windward plane of symmetry ($\theta = 0$), the strong divergence of the potential-flow streamlines would be expected to lead to a greater divergence of the

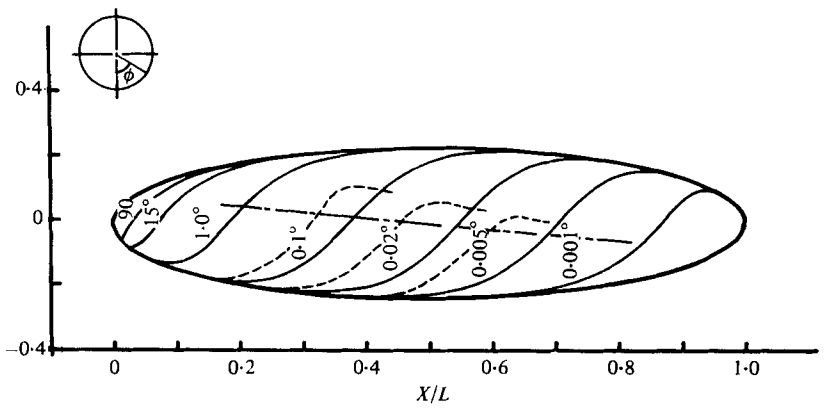

FIGURE 2. Streamlines on a 4·3:1 spheroid at 30° incidence. ——, potential-flow streamlines; – – –, surface streamlines; —·—, line of minimum pressure; ϕ = polar streamline angle at stagnation point.

surface streamlines and this would be accompanied by a thinning of the boundary layer. In proceeding towards the tail along the windward side, the prolonged favourable pressure gradient would tend to maintain a thin boundary layer and consequently delay the occurrence of reverse flow, i.e. singular separation, relative to the location of axisymmetric separation at zero incidence. Along the leeward plane of symmetry, on the other hand, the potential-flow pressure distribution would imply an accumulation of low-momentum fluid in the boundary layer with rapid thickening of the layer and earlier separation.

In the region away from the plane of symmetry, the pressure distribution and the curvature of the potential-flow streamlines enable us to infer the general direction of the surface streamlines. These are shown by the dashed lines in figure 2. Beyond the minimum pressure line, which is also shown, the circumferential flow encounters an adverse pressure gradient and, at some point, it would not be able to proceed towards the leeward side. The surface streamlines would begin to turn away from the leeward side ahead of such points. This 'reversal' of the circumferential flow leads to two secondary consequences. First, it would change the flow along the leeward plane of symmetry from being convergent to being divergent, at least in regions somewhat removed from the nose. This, in turn, would influence the growth of the boundary layer and its separation on the leeward side. Second, for sufficiently large angles of attack, the surface streamlines may merge into a line, as depicted in figure 2, which could be identified as an open or free-vortex separation line, discussed earlier. The origin of such a line remains uncertain, but it is characterized by streamlines coming together from both sides, leaving the surface and rolling up to form a longitudinal vortex.

In what follows, the various flow features noted here will be illustrated by means of a series of photographs taken during the flow-visualization study. These are also depicted in sketches based on the photographs and detailed observations recorded in a movie. Finally, the results are compared with previous experimental and theoretical evidence.

3. Flow-visualization studies

A 16 in. long spheroid with an axis ratio of 4·3 was fabricated from seasoned wood and was fitted with six small ports at $X/L = 0{\cdot}1$, where X is the axial distance from the nose and L is the total axial length of the model. Dye could be inserted into the model through a tube fitted into the nose and ejected from the surface through the six interconnected ports.

The model was mounted initially in a 30×36 in. hydraulic flume by means of eight support wires, four at the nose and four at the tail. The wires were provided with screw couplings so that their length could be adjusted to locate the model in any desired position.

Triple-strength blue and red food-colouring dye was used to visualize the flow pattern on the model surface. The dye was injected under gravity through the nose. However, in some instances, additional features of the flow were made visible by introducing dye of a different colour at appropriate places by hand using a long slender tube. The observations were recorded photographically and later filmed. All photographs were taken through the glass side wall of the flume. Consequently, in order to depict the flow on the windward, leeward and flank sides of the model at each incidence, it was necessary to realign the model in the flume.

The results obtained in the flume all correspond to a Reynolds number, based on the length of the model, of 8×10^4. The boundary layer in these tests is therefore expected to be laminar everywhere. Since higher Reynolds numbers could not be achieved readily in the flume, some additional tests were made by mounting the same model in a 30×36 in. wind-tunnel and visualizing some of the gross features of the flow by means of wool tufts attached to the model surface. It was, of course, not possible to reproduce the low Reynolds numbers of the flume in the wind tunnel, but observations could be made over a range of Reynolds numbers. Indeed, at the lowest wind-tunnel Reynolds number of $2{\cdot}5 \times 10^5$, which is still high compared with that used in the flume, some of the features of the laminar flow observed in the flume could be reproduced. The tests at the higher Reynolds numbers, up to 7×10^5, however, correspond to a turbulent boundary layer over most of the model.

3.1. *Axisymmetric flow* ($\alpha = 0$)

At zero incidence ($\alpha = 0$), the boundary layer is axisymmetric and separation is well defined. Figure 3 (plate 1) shows the corresponding surface streamlines. It is seen that separation occurs around $X/L = 0{\cdot}80$ and that the flow features are basically the same as those in two-dimensional flow. In the terminology of three-dimensional separation, this can be classified as singular or bubble-type separation (Maskell 1955) or closed separation (Wang 1972).

3.2. *Low incidence* ($\alpha = 5°$)

Figure 4 (plate 2) shows the surface streamlines on the spheroid at an incidence of 5° and a Reynolds number of 8×10^4. Three views are shown, namely the leeward side (top view), the flank of the body (side view) and the windward side (bottom view). The reversed flow near the tail has been made visible by injecting the red dye at the tail.

From figure 4(*c*), it is evident that there is a well-defined point of flow reversal on the windward plane of symmetry at about $X/L = 0{\cdot}84$, i.e. a little downstream of the point of axisymmetric separation noted earlier. As expected, the surface streamlines on either side of this plane are divergent up to the point of flow reversal.

On the flank of the body (figure 4*b*), the surface streamlines converge from the windward to the leeward side. This is in accordance with the expectation from the potential-flow pressure distribution. However, it is interesting to note the downward deflexion of the streamlines from about $X/L = 0{\cdot}55$, which implies a reversal of the circumferential component of velocity.

On the leeward plane of symmetry, the streamlines initially converge and then diverge, but the clarity of figure 4(*a*) is not sufficient to indicate the flow features near the tail. This is mainly due to the circumferential diffusion of the dye introduced upstream. The body was therefore turned around so that the dye ports lay near the tail, at $X/L = 0{\cdot}9$, and the photographs were taken again. These views, shown in figure 5 (plate 3), confirm the earlier observations and, in addition, indicate that the boundary layer on the leeward plane of symmetry also encounters flow reversal at approximately $X/L = 0{\cdot}94$, which is significantly downstream of the point of flow reversal on the windward side.

An attempt has been made in figure 6 to sketch the basic features observed from the photographs and introduce some detail. The points of flow reversal on the plane of symmetry ($S1$ and $S2$) are shown as singular saddle points of separation. The curved dashed line joining these two points (figure 6*b*) divides the flow coming from the upstream attachment point A from that which appears to originate from a downstream attachment point B. This is therefore a closed or bubble-type line of flow separation.

Now, since the flow from the saddle points $S1$ and $S2$ diverges and appears to run along the closed separation line, there must exist a singular nodal point of separation, such as $N1$, towards which the flow converges. Together with a singular nodal point on the other side of the body, there are now four singular points on the closed separation line. On the body as a whole, there are four nodal points (A, B, $N1$, and $N2$) and two saddle points ($S1$ and $S2$) on the surface. Thus the topological law referred to by Lighthill (1963), namely that the number of nodal points must exceed the number of saddle points by two, is also satisfied.

3.3. *Moderate incidence* ($\alpha = 10°$)

The observed flow patterns at an incidence of 10° are shown in figures 7 and 8 (plates 4 and 5). From the former it is clear that increased incidence leads to greater divergence of the flow from the windward plane of symmetry and greater convergence into the leeward plane over the nose region. Second, the streamline divergence from the leeward plane appears to start earlier ($X/L \sim 0{\cdot}45$) and leads to merging of the streamlines coming from the windward and leeward sides. The line along which this merging occurs is identified as an open separation line. Indeed, figure 7(*a*) and (*b*) show some evidence of the tendency of the boundary layer to roll up into a longitudinal vortex along this line. This particular feature was most clearly illustrated in the motion pictures. Owing to the inherent unsteadiness of the flow in this region, however, little could be said about the precise origin of the vortices or their relative size and strength. Figure 8 confirms the existence of reversed flow in the tail region.

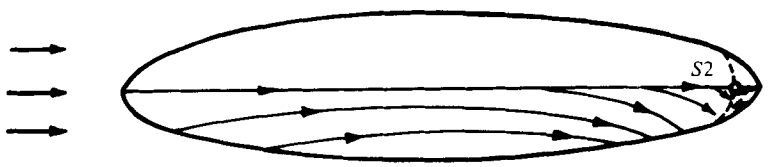

(*a*)

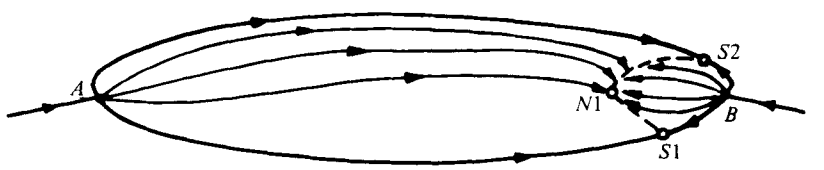

(*b*)

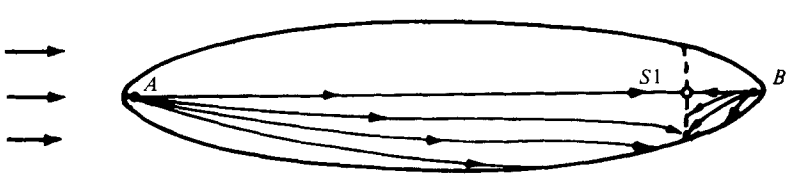

(*c*)

FIGURE 6. Surface flow pattern at low incidence ($\alpha = 5°$): (*a*) top view; (*b*) side view; (*c*) bottom view. ——, surface streamlines; – – –, closed separation.

The main features of the surface flow observed from several photographs are again depicted in the sketches in figure 9. Two nodal points ($N1$, and $N2$ on the opposite side of the body) have been added for reasons discussed earlier. Although very little direct experimental evidence is available either from previous work or the present photographs, it appears reasonable to assume that the nodal points of separation coincide with the intersections of the lines of open and closed separation. This is shown in figure 9(*b*).

3.4. *High incidence* ($\alpha = 20°, 30°, 40°$)

The photographs taken at an incidence of 20° are shown in figure 10 (plate 6), while those corresponding to 30° are shown in figure 11 (plate 7). It is seen from the former that the basic flow features at $\alpha = 20°$ and 30° are quite similar to those discussed

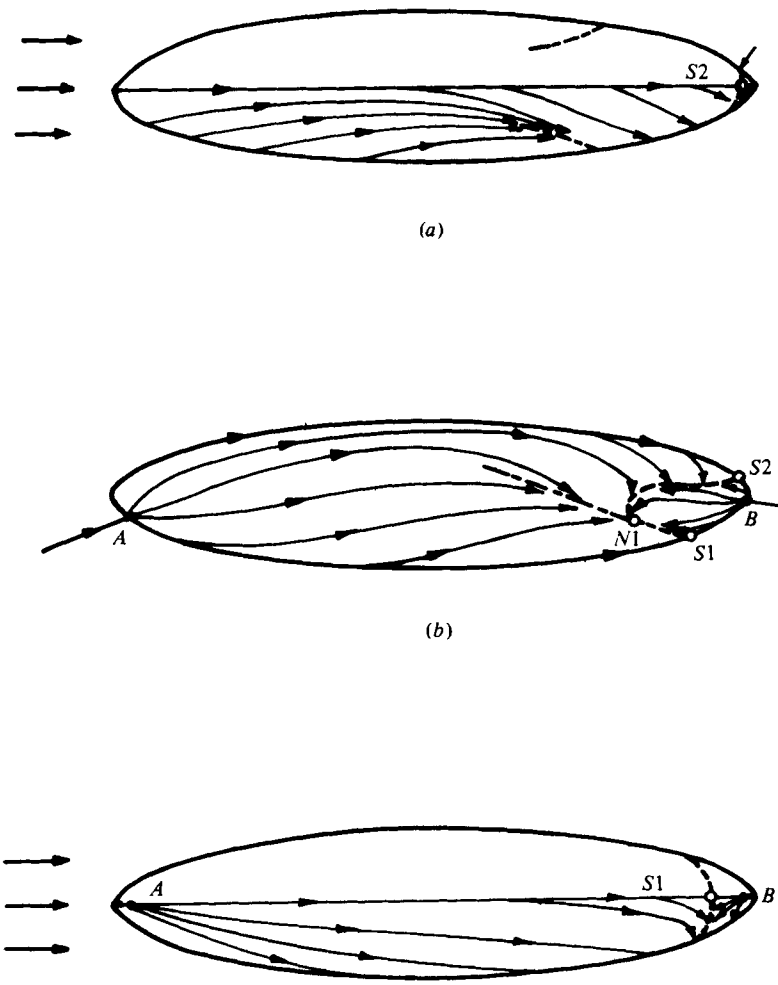

FIGURE 9. Surface flow pattern at moderate incidence ($\alpha = 10°$): (*a*) top view; (*b*) side view; (*c*) bottom view). ——, surface streamlines; – – –, closed separation; —·—, open separation.

earlier for $\alpha = 10°$. However, a more careful examination of these figures, in conjunction with similar photographs taken at other times and the observation of the actual flow in the flume, indicates that a new phenomenon occurs at these high incidences, namely the existence of a secondary open type of separation and reattachment. This is apparent from figure 11, corresponding to $\alpha = 30°$, and particularly in figure 12 (plate 8), which was taken by injecting a puff of red dye near the model nose with an incidence of 40°. Figures 11 (*b*) and 12 show three different lines running down the side of the model, the lowest one corresponding to the primary open separation, the top one corresponding to a secondary open separation, and the middle one indicating an open type of reattachment.

Since the open separation lines are characterized by convergence of surface stream-

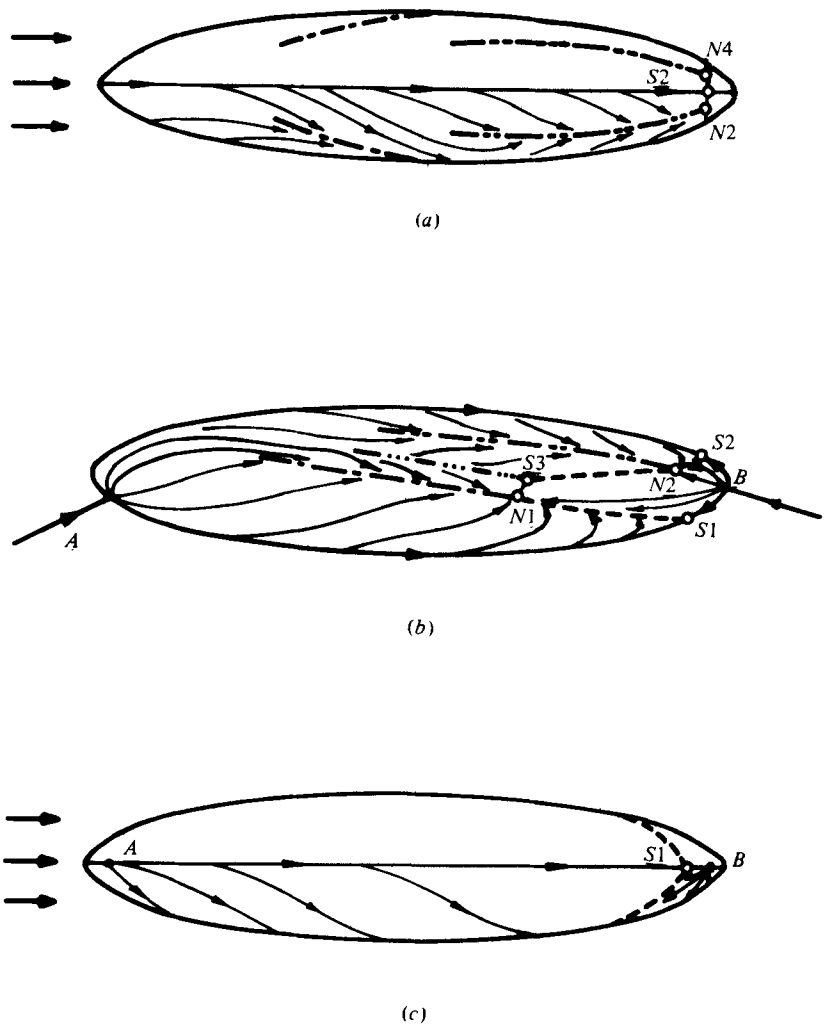

FIGURE 13. Surface flow pattern at high incidence ($\alpha \sim 30°$): (*a*) top view; (*b*) side view; (*c*) bottom view. ——, surface streamlines; – – –, closed separation; —·—, primary open separation; -···-, open reattachment; —··—, secondary open separation.

lines into them, the open reattachment line located between them is identified by the divergence of the streamlines emanating from it. This and other features of the flow at high incidences are illustrated in figure 13. Again it is postulated that the lines of open separation terminate at singular nodal points of separation $N1$ and $N2$ on the closed separation line, and correspondingly, that the open reattachment line terminates at the singular saddle point of separation $S3$, also located on the closed separation line. Thus there are now six nodal points and four saddle points on the surface, as required by the topological law.

Finally, it is seen from figures 10 and 11 that the region of reversed flow grows in extent as the incidence increases. It appears that, at large incidences, the reversed flow penetrates upstream for considerable distances along the side of the body but

remains anchored near the tail on the plane of symmetry. Although figure 11 indicates that two pairs of longitudinal vortices emanate from the lines of open separation and leave the surface (note the swirl and locations of the blue dye streaks), the resolution of the photographs was not good enough to either confirm or invalidate the various attempts that have been made to model such vortices. However, the existence of two pairs of vortices associated with two lines of open separation and one of open reattachment is compatible with a schematic interpretation by Thwaites (1960) of some earlier experimental observations. In the present case, the primary vortices on the sides of the body appear to be larger than those depicted by Thwaites (figure IX.22). Some indication of the size of the vortices on either side of the leeward plane of symmetry can be obtained from figure 14 (plate 8), which shows that dye injected at a point some distance away from the body on the plane of symmetry gets rapidly entrained towards the surface and into the vortices.

3.5. *Influence of Reynolds number*

As mentioned earlier, the spheroid was also tested in a wind tunnel over a range of Reynolds numbers in order to study turbulent separation. At the lowest Reynolds number of $2{\cdot}5 \times 10^5$, the flow patterns at all incidences were found to be quite similar to those observed in the flume and discussed above. As the Reynolds number was increased slightly over this value, however, the flow changed abruptly, but did not change thereafter with further increases in Reynolds number up to $7{\cdot}0 \times 10^5$, the maximum value obtained in the tunnel. Figure 15 (plate 9) shows the flow at a Reynolds number of $7{\cdot}0 \times 10^5$ at three different incidences. In view of the above observations, it was assumed that these correspond to a turbulent boundary layer over most of the body. Among the main features depicted by these photographs are the following. In axisymmetric flow ($\alpha = 0$), the location of separation is delayed to about $X/L = 0{\cdot}95$, which is considerably downstream of the point of laminar separation, $X/L = 0{\cdot}80$. At high incidences ($\alpha = 20°, 40°$), the wool tufts indicate an open type of separation along the side of the model. The line of open separation moves upstream as the incidence increases. There is also some evidence of a closed separation occurring near the tail. This method of flow visualization is not as satisfactory as dye in water and certainly does not give any evidence of the existence of any secondary separation at high incidences and low Reynolds numbers. Nevertheless, from the limited results presented here, it was concluded that the Reynolds number (and therefore the state of the boundary layer, i.e. laminar or turbulent) plays a significant role in the determination of the overall flow pattern on a spheroid at incidence. However, the qualitative features of open and closed separations, when they do occur, are similar for both laminar and turbulent flows.

4. Discussion

Laminar flow past a spheroid at incidence has also been examined by Wilson (1971). He used smoke to visualize the flow and made some measurements in the boundary layer along the leeward plane of symmetry. Wang has studied the problem computationally. He obtained numerical results first (1970, 1974*a*) for the boundary layer along the plane of symmetry and then (1974*b*, *c*, 1975) in regions removed from it.

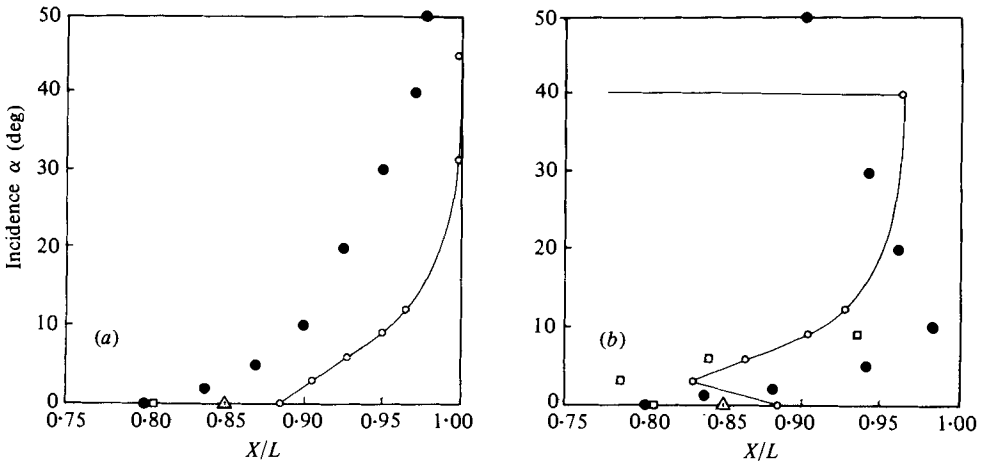

FIGURE 16. Location of singular separation points on the plane of symmetry: (*a*) windward side; (*b*) leeward side. ●, Present observations; △, calculation, Chang & Patel (1975); —○—, calculation, Wang (1972); □, experiment, Wilson (1971).

It should be pointed out that the experiments of Wilson and most of the computations of Wang correspond to a spheroid of axis ratio 4·0, whereas the present experiments employed a slightly more slender spheroid of axis ratio 4·3. This difference should be borne in mind in the comparisons made below.

Figure 16 shows the locations of the points of flow reversal ($S1$ and $S2$) on the windward and leeward sides of the plane of symmetry deduced from the photographs taken during the course of the present study. These are compared with the observations of Wilson and the calculations of Wang.

From figure 16(*a*) it is evident that the variation with incidence of the observed point of singular separation on the windward side is in qualitative agreement with the predictions of Wang. There is, however, a consistent and substantial discrepancy in the precise location which is not explained either by the small difference in the axis ratio or by possible effects of free-stream turbulence in the experiments, which was undoubtedly present. Some of the discrepancy may be attributed to the use of the potential-flow pressure distributions in the calculations since the actual pressure distribution may be significantly influenced by the complex flow pattern elsewhere on the body, at least at large incidences. This does not, however, explain the equally large discrepancy in axisymmetric flow ($\alpha = 0$), where the present observations are in excellent agreement with the experiments of Wilson and closer to the results of the computations made by Chang & Patel (1975) using two different methods and the potential-flow pressure distribution.

From the corresponding results presented in figure 16(*b*) for the leeward plane of symmetry, it is evident that the present observations are at variance with those of Wilson and the calculations of Wang. The influence of flow separation on the pressure distribution along the leeward side is expected to lead to quite substantial departures from the potential-flow solution used in the calculations, and consequently the disagreement between the experiment and the computations of Wang is not altogether surprising. It is of interest to note that the present results indicate a downstream movement of singular separation with increasing incidence up to about 10–15°. The

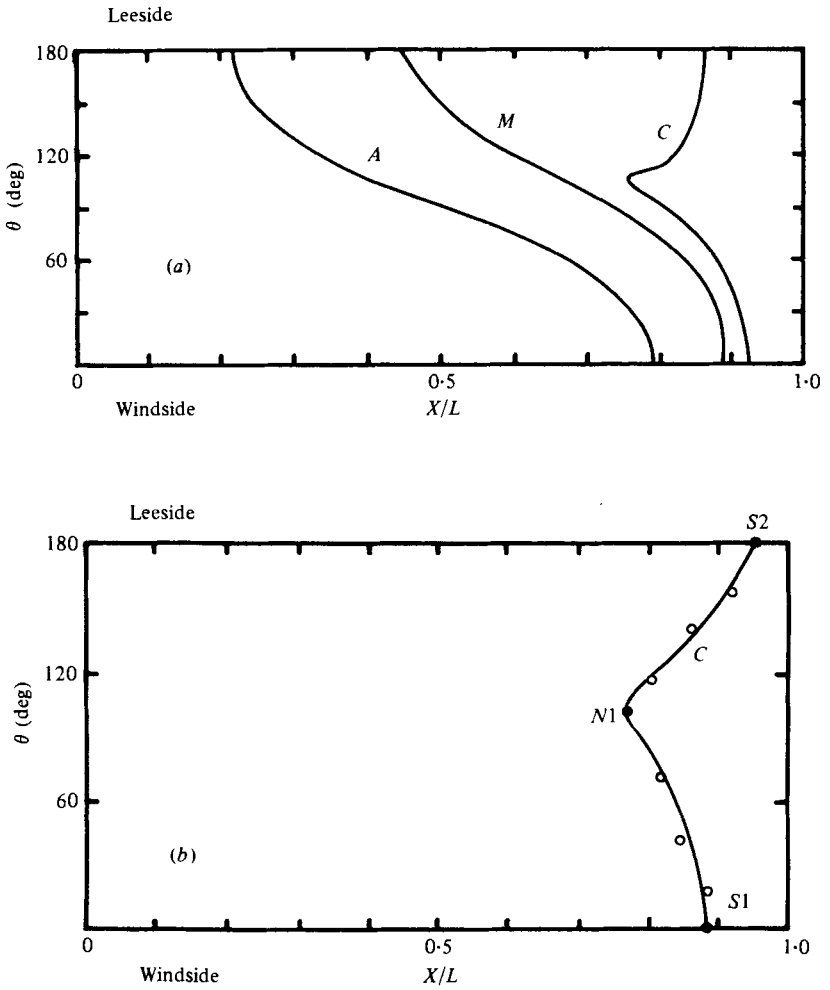

FIGURE 17. Comparison between calculation and observations at low incidence: A, minimum potential flow pressure line; M, locus of zero circumferential wall shear stress; C, closed separation. (a) Calculations, Wang (1974), $\alpha = 6°$; (b) From present photographs, $\alpha = 5°$.

trend is then reversed at higher incidences. It appears that this reversal in trend is associated with the onset of the secondary open separation, and corresponding reattachment, since this phenomenon was observed to take place between $\alpha = 10$ and 20°.

Figure 17 shows a comparison between the results of the more complete calculations of Wang (1974*b*, *c*), which included the off-symmetry plane regions, for a 4 : 1 spheroid at $\alpha = 6°$ and the present observations on the 4·3 : 1 spheroid at $\alpha = 5°$. It is seen that, at these low incidences, there is a remarkable qualitative agreement between the two sets of results with respect to the shape of the closed separation line, although, as discussed above, the locations of the singular separation points on the plane of symmetry are not predicted accurately.

A similar comparison is made in figure 18 for the higher incidence of 30°. Now it is seen that there is good agreement between the observed primary open separation line

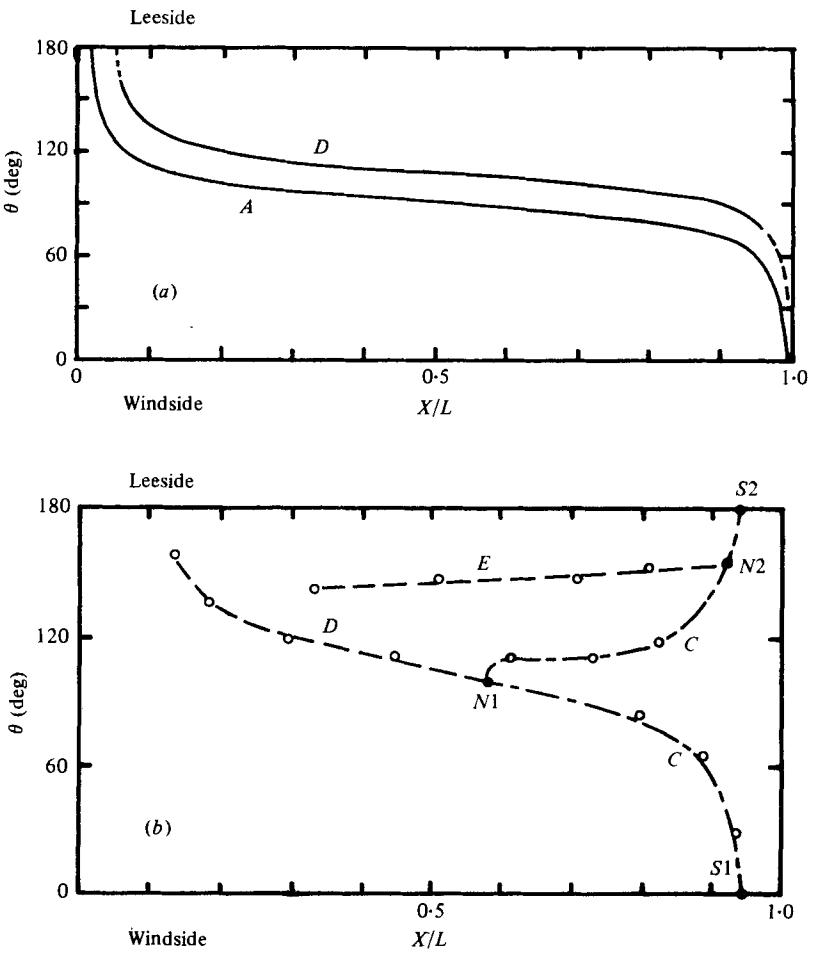

FIGURE 18. Comparison between calculation and observations at high incidence: A, minimum potential flow pressure line; C, closed separation; D, primary open separation; E, secondary open separation. (*a*) Calculation, Wang (1974), $\alpha = 30°$; (*b*) From present photographs, $\alpha = 30°$.

and that predicted by Wang. The position of this line relative to the locus of minimum potential-flow pressure coefficient is different in the two cases; this may be attributed to a strong interaction between the separated vortical flow and the external inviscid flow. The actual minimum pressure line must lie towards the windward side of the observed line of open separation. The numerical technique adopted by Wang was such that his boundary-layer calculation marched downstream and proceeded from the windward to the leeward side. However, the calculations could not be continued towards the leeward side beyond the line of primary open separation. Consequently, several important details of the observed flow, including the secondary open separation, reattachment and the closed separation could not be predicted. In fact, it is doubtful whether all of these could be predicted at all with the usual thin-boundary-layer formulation.

5. Conclusions

This visual study has helped to identify the basic features of three-dimensional boundary-layer separation on a body of revolution at incidence. Although the topology of the surface streamlines, or skin-friction lines, does not give a complete description of the overall viscous flow past the body, and its aerodynamic or hydrodynamic consequences, it nevertheless enables the identification of two basic types of three-dimensional flow separation: a closed or bubble type of separation and an open or free-vortex type of separation. Thus the proposals of Maskell (1955) and Wang (1972) are verified by the present experiments.

The results presented here also shed some light on the usefulness and limitations of boundary-layer theory in theoretical and experimental descriptions of the complicated flow past bodies of arbitrary shape. It will be apparent that careful and detailed measurements of the surface pressure distribution and boundary-layer development in the neighbourhood of open and closed separation lines are needed not only to establish quantitative separation criteria for incorporation in the newly emerging boundary-layer calculation procedures, but also to calibrate such procedures. Indeed, the present study has led to the design of such an experiment, which is now in progress. The observations made here concerning an open or free-vortex separation indicate that it should be possible to calculate the boundary-layer development on either side of it since the flow on both sides originates from the upstream stagnation point. The authors are not aware of a successful computation of this type in either laminar or turbulent flow. The formation of the vortex along the open separation line would, however, suggest that boundary-layer theory would break down over some region along and on either side of this line as the vortex ceases to be buried inside the boundary layer and leaves the surface. This breakdown is expected to be gradual and not catastrophic since the boundary-layer equations are not singular there. It is obvious that these ideas need to be confirmed by both experiments and computations. Calculations in regions downstream of the closed separation line are obviously beyond the scope of boundary-layer theory. However, studies of the type discussed here would indicate the limitations of boundary-layer theory, lead to a better understanding of the interaction between the viscous (boundary-layer and vortex) flow and the external inviscid flow, and suggest ways in which such a coupling could be established in computation procedures. Finally, it is interesting to note that the formation of longitudinal vortices from open separation may explain the origin of bilge vortices observed on certain ship forms where the shape is such as to lead to rapid changes in the curvature of the inviscid streamlines, similar to those present over the nose of a blunt body of revolution at incidence. The observed dependence on incidence of the locations of the flow reversal points on the plane of symmetry also has an important bearing on the understanding of the flow along the keel of a ship form and on the plane of symmetry of aircraft fuselages and similar shapes at incidence.

This research was supported in part by Grant No. DAAG29-76-G-0036 from the U.S. Army Research Office. Partial support was also provided in the later stages of the study by the Lockheed–Georgia Company. The authors are grateful to Professors L. Landweber and B. R. Ramaprian for many helpful discussions during the course of the study.

REFERENCES

CHANG, K. C. & PATEL, V. C. 1975 Calculations of three-dimensional boundary layers on ship forms. *Iowa Inst. Hydraul. Res., Univ. Iowa, IIHR Rep.* no. 178.

HAN, T. & PATEL, V. C. 1977 Flow visualization of three-dimensional boundary-layer separation on bodies of revolution at incidence. *Iowa Inst. Hydraul. Res., Univ. Iowa, IIHR Rep.* no. 205.

LIGHTHILL, M. J. 1963 *Laminar Boundary Layers* (ed. L. Rosenhead), pp. 46–113. Oxford: Clarendon Press.

MASKELL, E. C. 1955 Flow separation in three dimensions. *Brit. R.A.E. Rep. Aero* 2565.

STETSON, K. F. 1972 Boundary-layer separation on slender cones at angle of attack. *A.I.A.A. J.* **10**, 642–648.

THWAITES, B. (ed.) 1960 *Incompressible Aerodynamics*. Oxford University Press.

WANG, K. C. 1970 Three-dimensional boundary layer near the plane of symmetry of a spheroid at incidence. *J. Fluid Mech.* **43**, 187–209.

WANG, K. C. 1972 Separation patterns of boundary layer over an inclined body of revolution. *A.I.A.A. J.* **10**, 1044–1050.

WANG, K. C. 1974*a* Laminar boundary layers near the symmetry-plane of a prolate spheroid. *A.I.A.A. J.* **12**, 949–958.

WANG, K. C. 1974*b* Boundary layer over a blunt body at high incidence with an open-type of separation. *Proc. Roy. Soc.* A **340**, 33–55.

WANG, K. C. 1974*c* Boundary layer over a blunt body at extremely high incidences. *Phys. Fluids* **17**, 1381–1385.

WANG, K. C. 1975 Boundary layer over a blunt body at low incidence with circumferential reversed flow. *J. Fluid Mech.* **72**, 49–65.

WANG, K. C. 1976 Separation of three-dimensional flow. *Rev. Viscous Flow, Proc. Lockheed-Georgia Co. Symp.* pp. 341–414.

WILSON, G. R. 1971 Experimental study of a laminar boundary layer on a body of revolution. M.Sc. thesis, Air Force Inst. of Tech., Wright-Patterson AFB, no. GAM/AE/71-4.

ZAKKAY, V., MIYAZAWA, M. & WANG, C. R. 1974 Lee surface flow phenomena over space shuttle at large angles of attack at $M_\infty = 6$. *N.A.S.A. Contractor rep.* no. 132501. (See also *A.I.A.A. Paper* no. 71–548, 1975.)

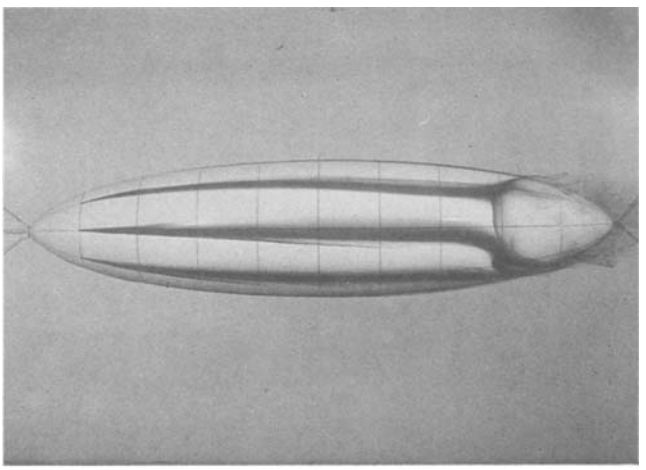

FIGURE 3. Flow pattern at zero incidence.

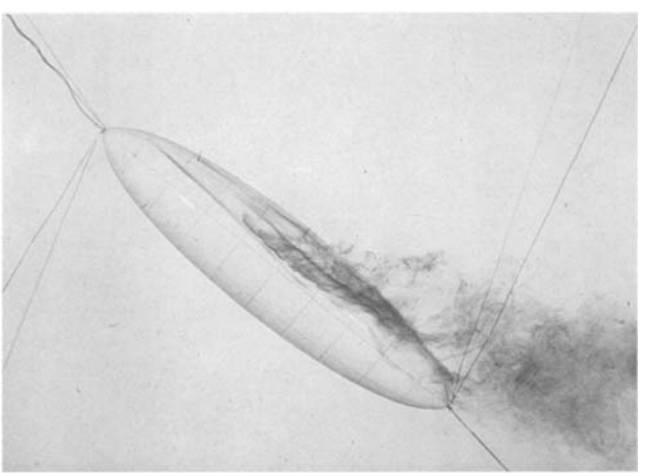

FIGURE 12. Primary and secondary open separations and reattachment at $\alpha = 40°$.

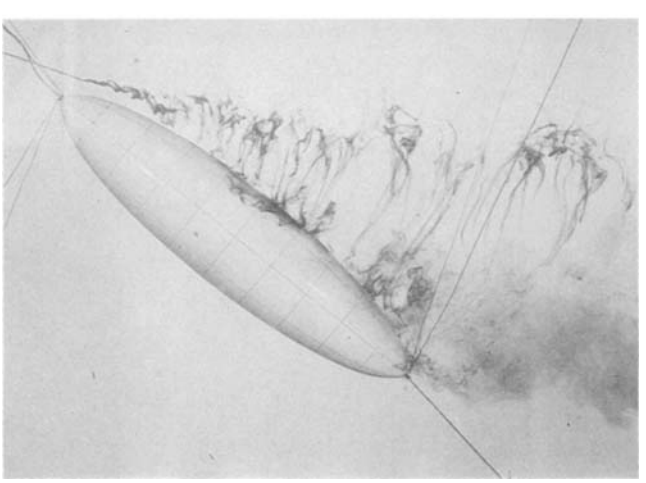

FIGURE 14. Entrainment into the leeward plane of symmetry ($\alpha = 40°$).

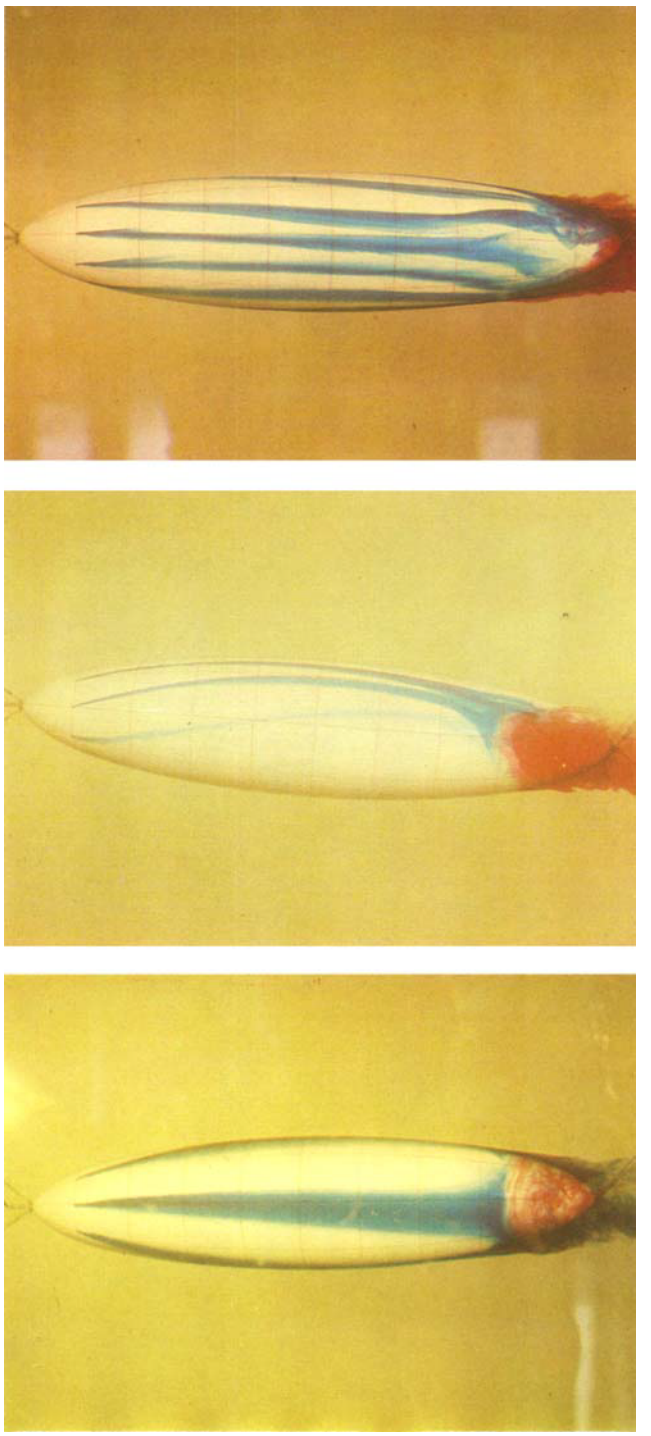

FIGURE 4. Flow pattern at $\alpha = 5°$: (*a*) top (leeward) view; (*b*) side view; (*c*) bottom (windward) view.

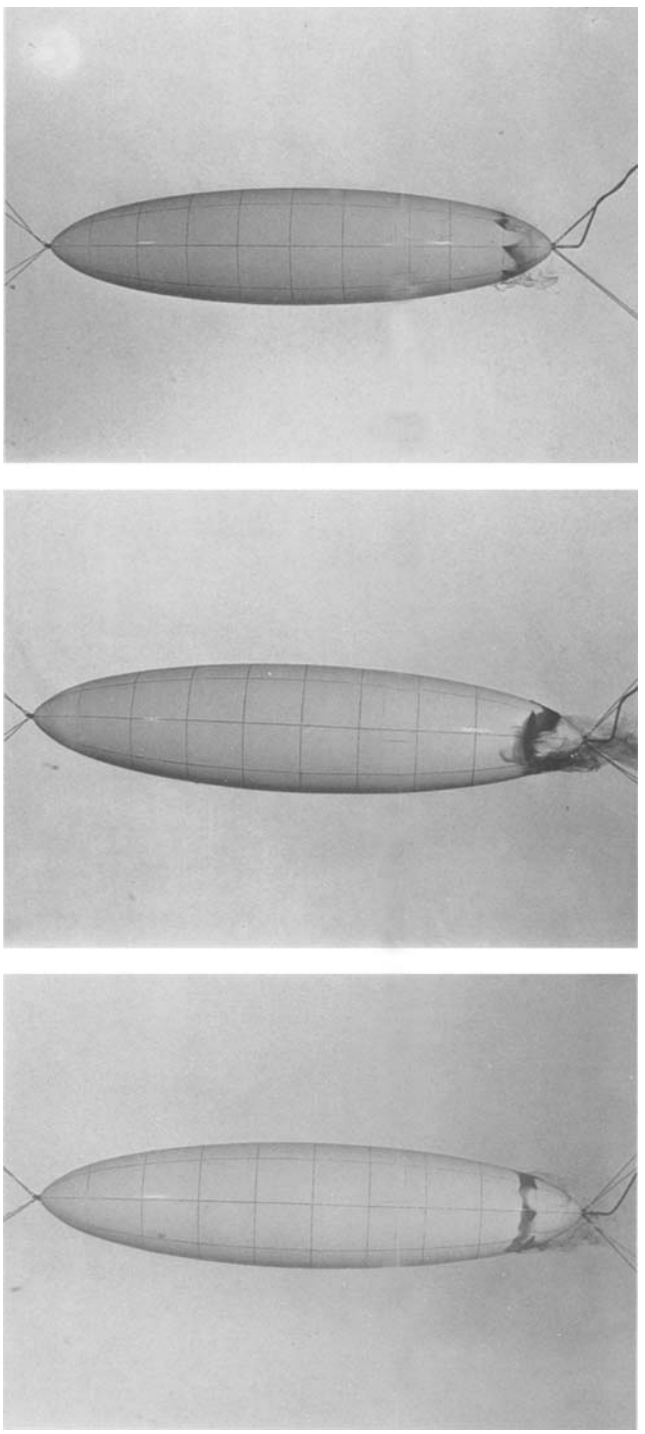

FIGURE 5. Details of flow near the tail at $\alpha = 5°$:
(*a*) top view; (*b*) side view; (*c*) bottom view.

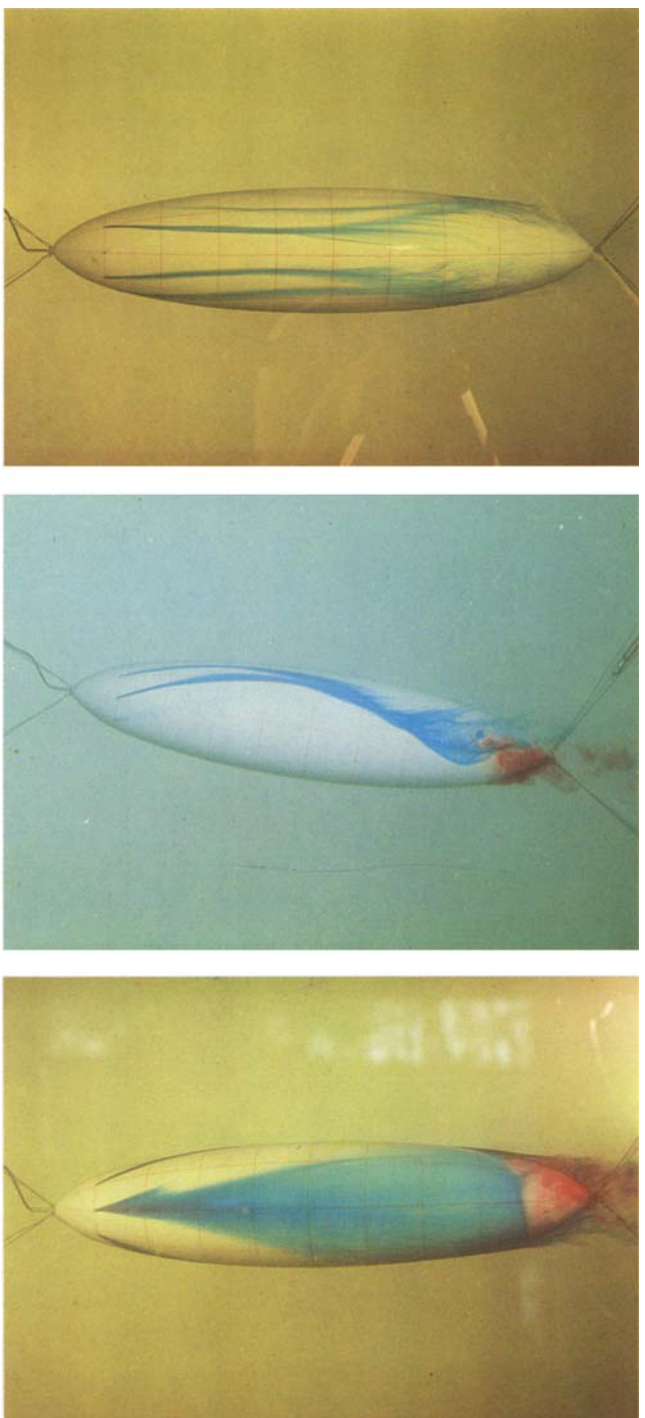

FIGURE 7. Flow pattern at $\alpha = 10°$: (*a*) top view; (*b*) side view; (*c*) bottom view.

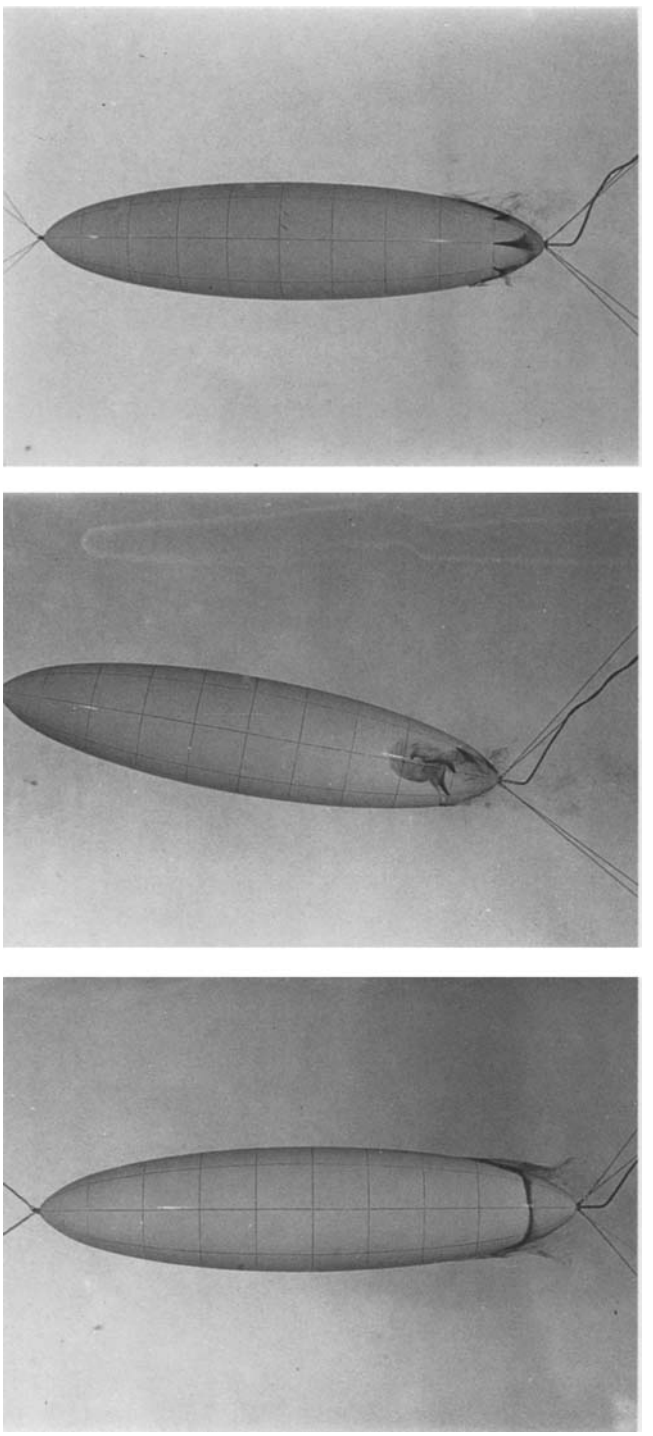

FIGURE 8. Details of flow near the tail at $\alpha = 10°$:
(*a*) top view; (*b*) side view; (*c*) bottom view.

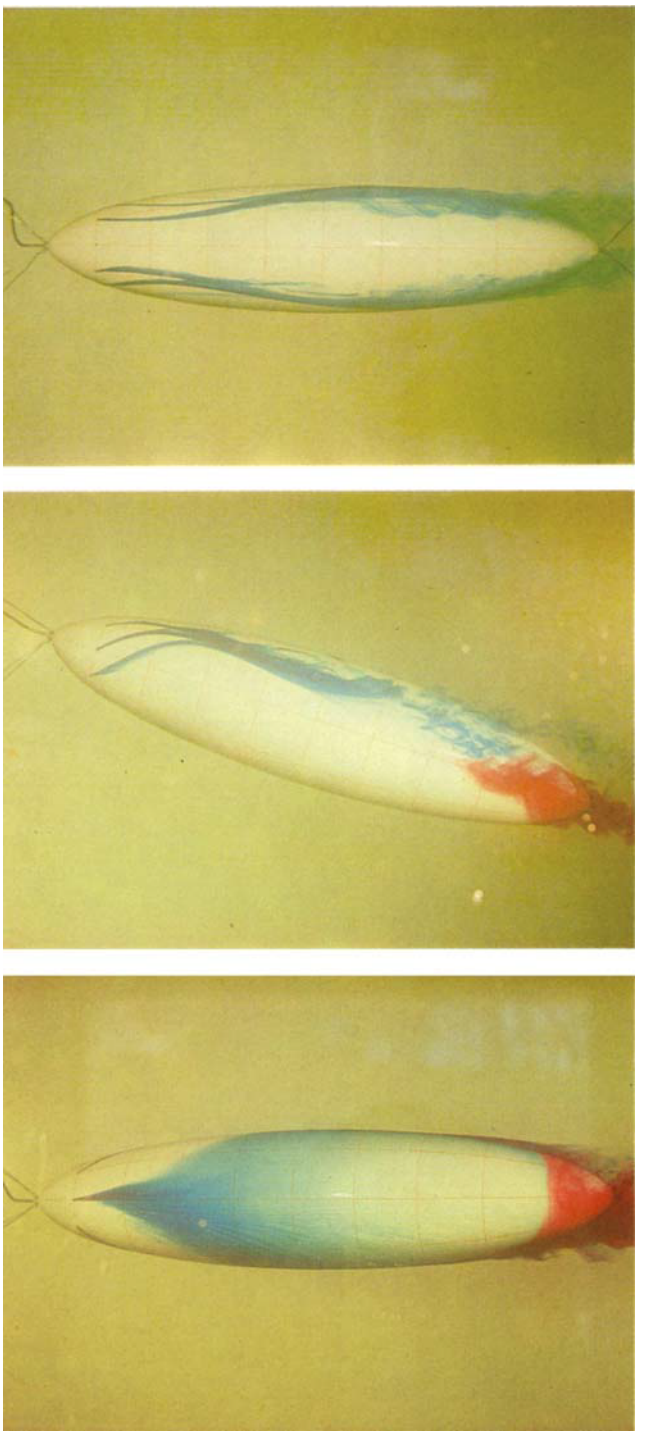

FIGURE 10. Flow pattern at $\alpha = 20°$: (*a*) top view; (*b*) side view; (*c*) bottom view.

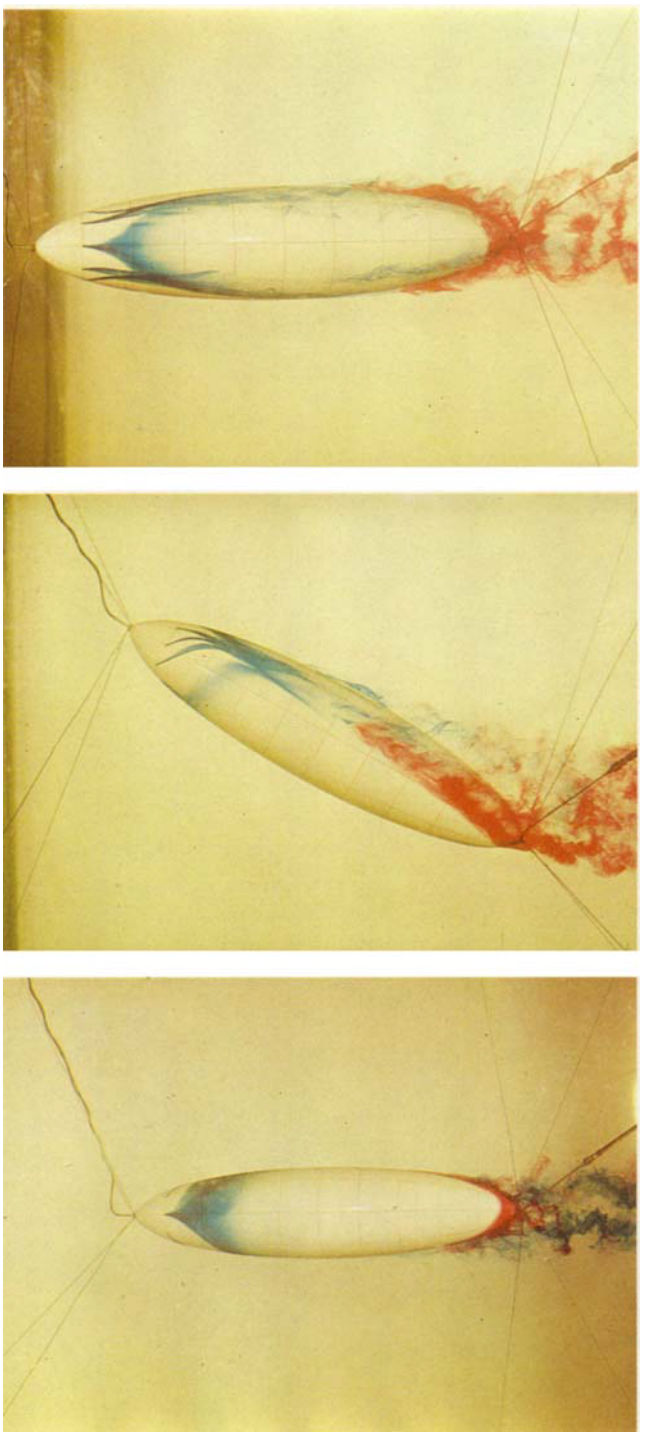

FIGURE 11. Flow pattern at $\alpha = 30°$: (*a*) top view; (*b*) side view; (*c*) bottom view.

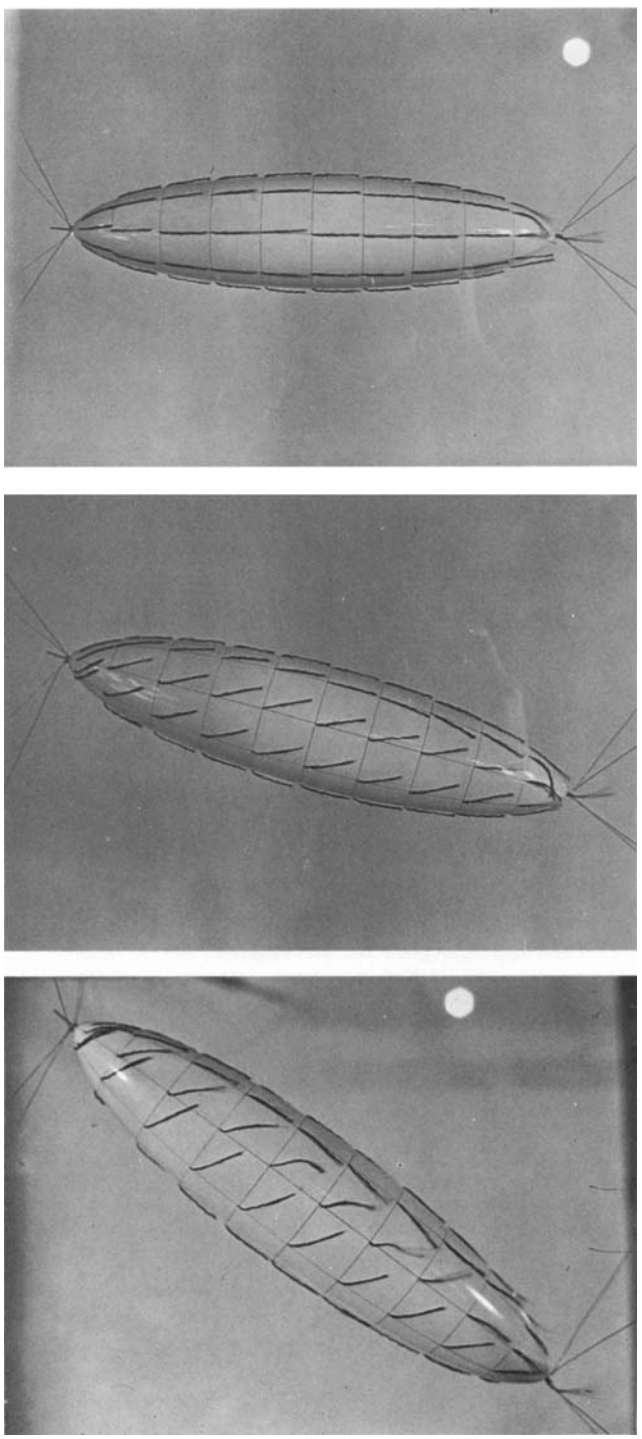

FIGURE 15. Wind-tunnel observations at a Reynolds number of 7×10^5: (*a*) axisymmetric flow; (*b*) $\alpha = 20°$, side view; (*c*) $\alpha = 40°$, side view.